Chapter 7

Ru(III) benzothiazole Schiff base complexes

7.1. Introduction

The chemistry and biological study of heterocyclic compounds has been an interesting and remarkable field for a long time in medicinal chemistry. A number of heterocyclic derivatives containing nitrogen and sulphur atom serve as unique and versatile scaffolds for drug design[1]. Benzothiazole is one of the most important heterocycle which contains thiazole ring fused with benzene ring with diversified molecular design and remarkable optical, liquid and electronic properties[2]. A number of 2-aminobenzothiazoles were extensively studied as central muscle relaxants, glutamate neurotransmission inhibitor Riluzole (6-trifluoormethoxy-2-benzothiazolamines, Rilutek) since 1950. It has diverse chemical reactivity and broad spectrum of activity like antimicrobial[3], anti-inflammatory[4], anti-HIV activity[5], antileishmanial agents[6], antitubercular[7], antimalarial[8], analgesic[9], anticonvulsant[10], anticancer[11]and lipid peroxidation inhibitors[12]. These compounds serve as unique, versatile scaffolds for the development of newer drugs which may exhibit mechanism of action *via* diverse biological targets.[13-17.]

Benzothiazoles show chemotherapeutic activity and a considerable amount of work has been done on the synthesis of new potent antibacterial and antifungal benzothiazoles. 2-(substituted arylsulfonamido)benzothiazole have been reported for their anti-bacterial activity against *Bacillus subtilis, Salmonella typhi* and *S. dysentery.*

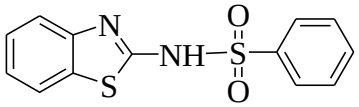

N-Benzothiazol-2-yl-benzenesulfonamide

The benzothiazole moiety with various substitutions has shown antitumor activity. The aminomethylphenyl derivatives and 4,7-dimethoxy benzothiazole shows selective growth inhibitory properties against human cancer cell lines and proliferation of cells respectively. Chlorinated and fluorinated derivatives of this moiety exhibit good *in vitro* as well as *in vivo* antitumor activity.

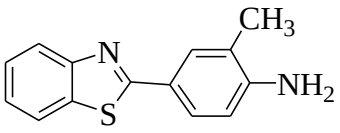

4-Benzothiazol-2-yl-2-methyl-phenylamine

Recent reports on the resistance of benzimidazoles have forced the researchers to develop new drugs with anthelmintic activity, to fight against helminthiasis, which is causing untold misery to the infected individuals. Benzothiazole derivatives have been synthesized, which is sulphur isostere of benzimidazole, reported for better anthelmintic activity.

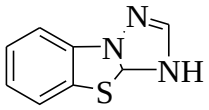

3,3a-Dihydro-benzo[4,5]thiazolo[3,2-b][1,2,4]triazole

Pyrazolones and pyrazolinones are more valuable non- steroidal anti- inflammatory agents. Phenylbutazone and its congeners incorporating a pyrazoline- 3, 5- dione structure are more potent anti- inflammatory agents. In the recent years a number of benzothiazole derivatives have been synthesized and found to possess anti- inflammatory activity. **Singh *et al.*,** synthesized and characterized some new 2- (4'- butyl- 3',5'- dimethylpyrazol - 1'- yl)- 6- substitutedbenzothiazole which were found to posses significant anti- inflammatory activity.

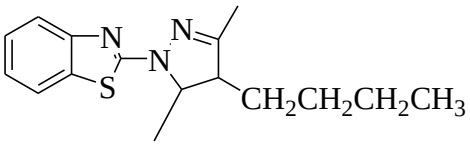

2-(4-Butyl-3,5-dimethyl-4,5-dihydro-pyrazol-1-yl)-benzothiazole

These compounds constitute bioactive pharmacore of many drugs and serve as versatile scaffolds for the development of newer drugs. Understanding the binding of the key components of nucleic acids like DNA-drug binding is very much essential for the identification of newer drugs[18, 19]. Thus benzothiazole is considered as a distinct class of chemotherapeutic agents in the literature. Our aim is to present a study on the pharmacological action of the Schiff bases derived from benzothiazole derivative and its complexes.

7.2. Synthesis of Schiff bases

A mixture of 2-amino-6-methyl-benzothiazole (0.16g, 1mmol), salicylaldehyde (0.12 ml, 1mmol) or 5-bromo salicylaldehyde (0.20g, 1mmol) in 95% ethanol was refluxed for 2h. The precipitate was filtered and washed with ethanol.

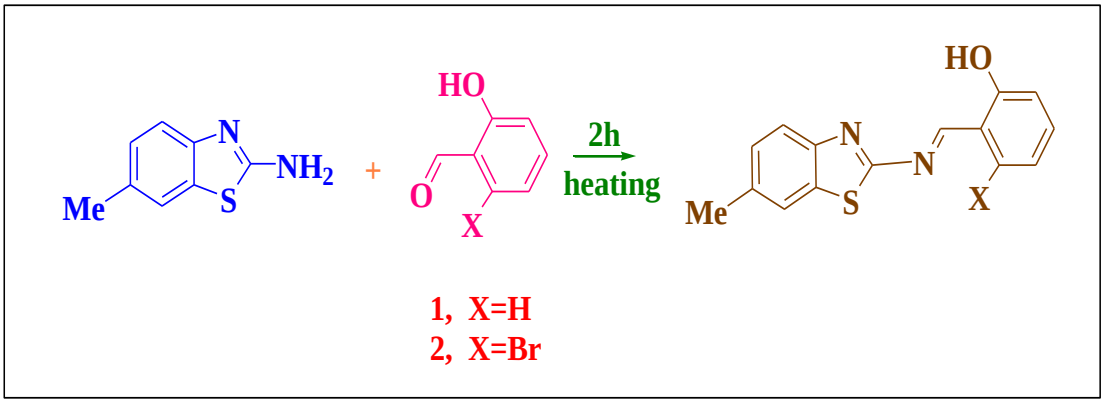

Scheme 1: Synthesis of Schiff base

7.2.1. *2-[6-Methyl-benzothiazol-2-ylimino)-methylphenol* (1) L^1 :

Crystallised from DMF/H_2O; yield 78%; mp: 237°C. Anal. calcd (%) for $C_{15}H_{12}N_2OS$ (268.33) C, 67.14; H, 4.51; N, 10.44; found (%), C, 67.05; H, 4.69; N, 10.56. IR(KBr, cm^{-1}): 3394 (-OH); 1596(>C=N); 1560(>C=N thiazole ring), 661 (C-S). λ_{max} (DMF, nm): 312, 368, 408. ^{1}H NMR (DMSO, ppm): 6.971-7.684(m, Ar-H), 2.495 (s, CH_3), 9.245(s, -CH=N), 5.031(s, -OH).

7.2.2. *3-Bromo-2-[6-methyl-benzothiazol-2-ylimino)-methylphenol* (2) L^2 :

Crystallised from DMF/H_2O; yield 75%; mp: 254°C. Anal. calcd. (%) for $C_{15}H_{11}BrN_2OS$ (347.23) C, 51.89; H, 3.19; N: 8.07; found (%), C, 51.72; H, 3.21; N: 8.64. IR(KBr, cm^{-1}): 3421 (-OH); 1591(-C=N); 1552 (-C=N thiazole ring), 675 (C-S). λ_{max}(DMF, nm): 315, 368, 395. ^{1}H-NMR(DMSO, ppm): 6.949-7.869(m, Ar-H), 2.497 (s, CH_3), 9.168(s, -CH=N), 5.437(s, -OH).

7.3. Synthesis of complexes

7.3.1. Synthesis of $[Ru(Cl)_2(PPh_3)(L^1)]$(3)

A methanolic solution (20 mL) containing L^1 **(1) (**1mmol) and $[RuCl_3(PPh_3)_3]$ (1mmol) in benzene (20mL) were mixed and the resulting brown solution was refluxed for 8 h (Scheme 2). The reaction mixture was then cooled to room temperature. The brown colored crystalline precipitate formed was filtered off and the purity was checked by TLC. This solid was crystallized from CH_2Cl_2/hexane mixture. Yield: 67%, mp: 268°C. Anal. calcd. for (%) $C_{33}H_{26}Cl_2N_2OSPRu$: C, 56.49; H, 3.74; N, 3.99; S, 4.57. found(%): C, 55.98; H, 3.75; N, 3.91; S, 4.53. EI-MS: Found

m/z = 701.60 (M^+); calcd. m/z=701.05(M^+). IR (KBr, cm^{-1}): 1539(C=N), 675(C-S-C). UV-vis (DMSO) λmax, nm: 280, 380, 413. EPR (300 K, g value): 1.99.

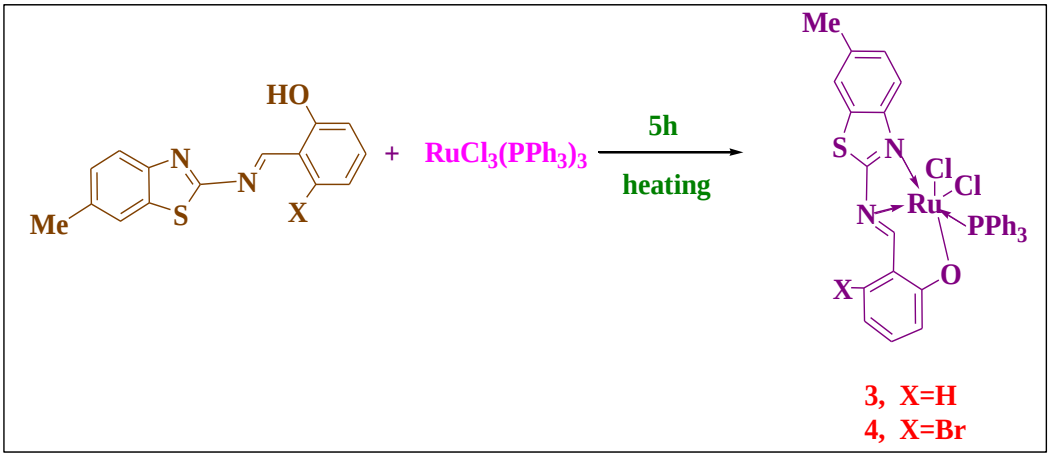

Scheme 2: Synthesis of complexes

7.3.2. Synthesis of $[Ru(Cl)_2(PPh_3)(L^2)]$(4)

It was prepared using the same procedure as described for **3** with L^2. Brown colored crystalline powder. Yield: 56%. mp: 274°C. Anal. calcd (%). for $C_{33}H_{25}Cl_2N_2OSPBrRu$: C, 50.78; H, 3.23; N, 3.59; S, 4.11. found (%): C, 50.71; H, 3.18; N, 3.50; S, 4.20. EI-MS: Found m/z= 781.13(M^+); calcd m/z=780.52(M^+). IR (KBr,cm^{-1}): 1568 (C=N), 673 (C-S). UV-vis (DMSO) λmax, nm: 285, 360, 408. EPR (300 K, g value): 2.12.

7.3.3. Structural description of Schiff base ligand

The single crystal XRD study of the Schiff base **1** reveals that it has the empirical formula $C_{15}H_{12}N_2OS$ with formula weight 268.33. It crystallizes in monoclinic crystal system with the space group P121/C1 with unit cell dimensions a=4.7851(2)Å, b=11.5926(4)Å, c=22.8100(7)Å , β=94.871(2)°. The bond lengths of S(1)-C(1), S(1)-C(8), O(1)-H(1), O(1)-C(11), N(1)-C(2), N(1)-C(8), N(2)-C(8), N(2)-C(9), C(1)-C(2), C(3)-H(3), C(7)-H(7A), C(7)-H(7B) are 1.7345(16), 1.7521(16), 0.8400, 1.351(2), 1.387(2), 1.297(2), 1.390(2), 1.301(2), 1.405(2), 0.9500, 0.9800, 0.9800Å respectively. The bond angles of C(1)-S(1)-C(8), C(11)-O(1)-H(1), C(8)-N(1)-C(2), C(9)-N(2)-C(8), C(2)-C(1)-S(1), N(1)-C(2)-C(3), C(5)-C(7)-H(7A), C(5)-C(7)-H(7B) are 88.72(8), 109.5, 109.89(13), 119.32(14), 109.16(11), 125.84(15), 109.5, 109.5° respectively. Hydrogen bonding is present in **1** between H(1)-N(2). The crystal data and the refinement parameters, selected bond angles and bond angles, hydrogen bond parameters are given in table 7.1-7.3 respectively. The ORTEP and

the packing diagram of the Schiff base ligand is shown in Fig. 7.1 and 7.2 respectively.

The ^{1}H-NMR spectrum of the Schiff bases were recorded in DMSO-*d*6 and the resonances are explained as follows. The resonance due to the hydroxyl proton in the ligand **1** and **2** was observed at δ 5.021 and δ 5.437 ppm, respectively, while the resonance due to the imine proton appeared at δ 9.245 and δ 9.168 respectively. The signals due to aromatic phenyl ring and the thiazole ring were observed as multiplets around δ 6.971 to δ 7.684 ppm. The methyl protons in the ligands show resonances at δ2.49 ppm. The ^{1}H-NMR spectra of the ligands are shown in Fig. 7.3 and 7.4 respectively.

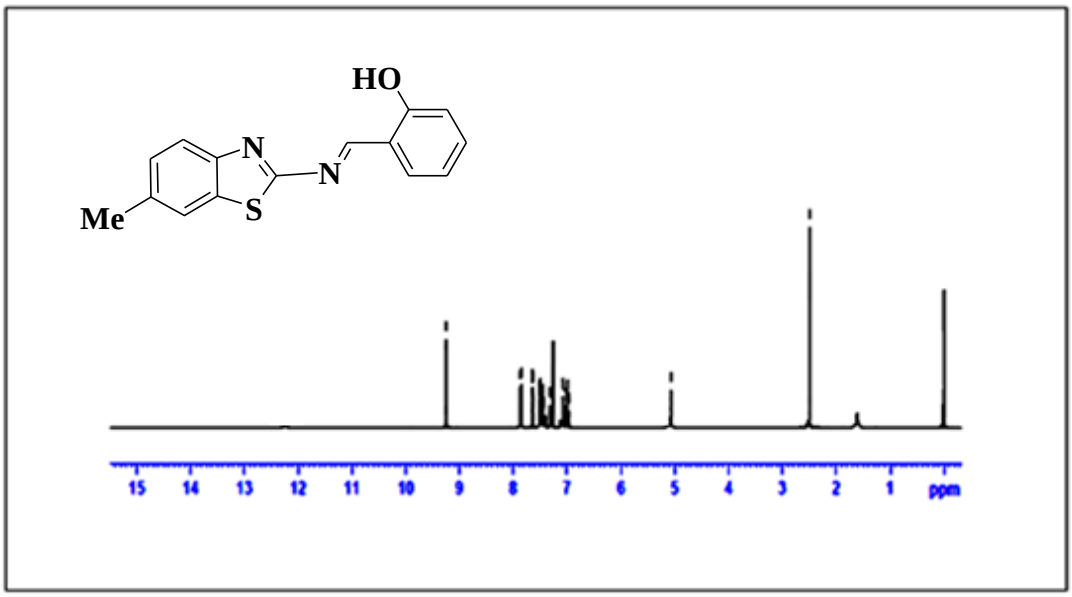

Fig. 7.3. ^{1}H-NMR spectrum of Schiff base 1

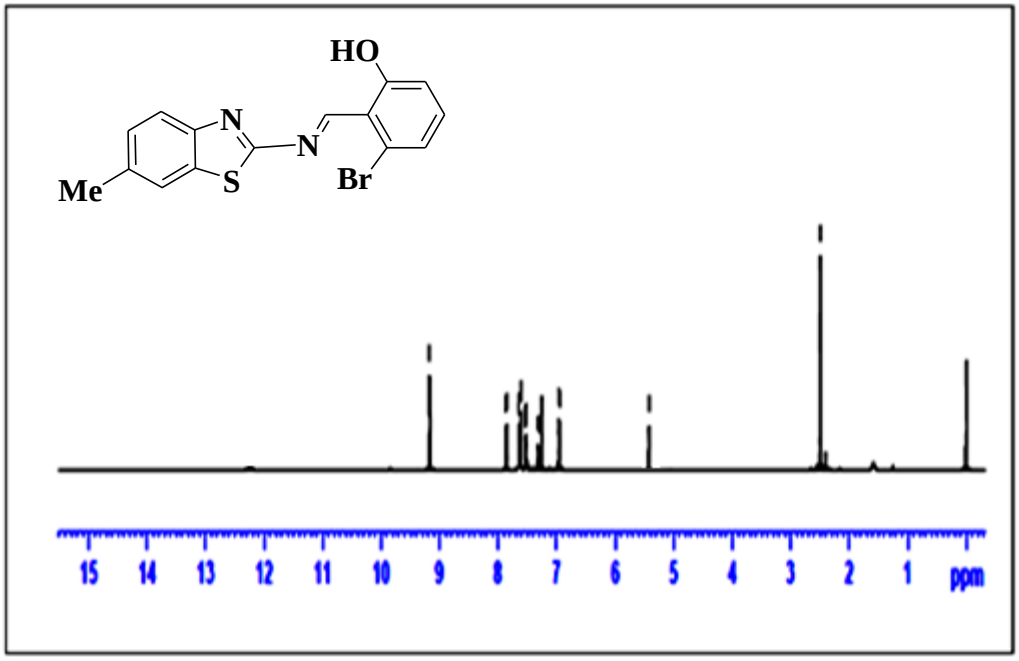

Fig. 7. 4. ^{1}H-NMR spectrum of Schiff base 2

7.3.4. FT-IR spectra

The IR spectral data for the Schiff base ligand and complexes are listed in Table 7.4. and the spectrum of the ligands and the complexes are shown in Figs. 7.5a – 7.5d respectively. The change in profile of stretching frequencies in the complexes, while compared with those observed for the isolated ligand confirms the coordination of the ligand with the central metal ion.

A broad strong absorption band observed at 3400-3350 cm^{-1} in the IR spectra of the ligands **1** and **2** is due to the stretching vibration of -OH group which disappears in the spectra of the complexes, indicating the deprotonation of the phenolic group and the coordination of these ligands through the phenolic oxygen. A strong band in the range 1591--1596 cm^{-1} due to the azomethine group (C=N) of free ligands was shifted to lower frequency in the spectra of complexes in the range 1539-1568 cm^{-1} indicating that the coordination is through azomethine nitrogen atom. IR spectra of the ligands revealed a medium intensity band in the region 1552-1560 cm^{-1} ν(C=N) thiazole ring, which is shifted to lower frequency in the range 1486-1494 cm^{-1} after complexation, which also indicates that it has been affected upon coordination to the metal ion. The ν(C-S-C) at 675 and 673cm^{-1} of the thiazole ring remains unchanged which demonstrated that the thiazole group of sulphur does not coordinate to the ruthenium metal. The C-O stretching frequency of the ligands range

between 1040 and 1045 cm^{-1} which is shifted to higher wavelengths in the complexes 1126 to 1139 cm^{-1} showing that the phenolic –OH is involved in co-ordination[18-20]. The ruthenium (III) Schiff base complexes show strong vibrations in the range 650-690, 1081-1105 and 1447-1450cm^{-1} which are attributed to the triphenyl phosphine fragments.

Table 7.4. FT-IR spectral data of the ligand and the complexes in cm^{-1}

Compound	ν(C-S-C)	ν(C=N)	ν(C=N)ring	ν(OH)	ν (C-O)
$C_{15}H_{12}N_2OS$	675	1596	1560	3324	1045
$C_{15}H_{11}N_2OSBr$	673	1591	1552	3345	1040
$[Ru(Cl)_2(PPh_3)(L^1)]$	675	1539	1486	-	1126
$[Ru(Cl)_2(PPh_3)(L^2)]$	673	1568	1494	-	1139

7.3.5. Electronic spectra

The ruthenium (III) complexes are paramagnetic in nature indicating the +3 oxidation state of ruthenium ion. The electronic spectra of the ligands in methanol show two bands in the regions 265-375 and 225–235 nm which corresponds to π–π*and n–π* transitions, respectively. The UV–vis spectra of the complexes **3** and **4** (Fig 7.6a and 7.6b) were recorded in CH_2Cl_2 which showed four bands in the region 210–400 nm. The bands below 300 nm can be attributed to intra-ligand transitions. The high intensity bands which appeared at 382 nm region have been assigned to L →M charge transfer bands arising due to the transitions from Cl and Br ligands to ruthenium. A weak band observed above 400 nm in the spectra of the complexes can be attributed to the d–d transitions.

Table 7.5. Electronic spectral details of the ligand and the complexes

Compound	Wavelength(nm)	Band assignments	Geometry
$C_{15}H_{12}N_2OS$	225, 265,370	π–π*, n–π*	-
$C_{15}H_{11}N_2OSBr$	235, 270,375	π–π*, n–π*	-
$[Ru(Cl)_2(PPh_3)(L^1)]$	280, 380, 413	Charge transfer, $^2T_{2g}\rightarrow{}^4T_{2g}$	Octahedral
$[Ru(Cl)_2(PPh_3)(L^2)]$	285,360, 408	Charge transfer, $^2T_{2g}\rightarrow{}^4T_{2g}$	Octahedral

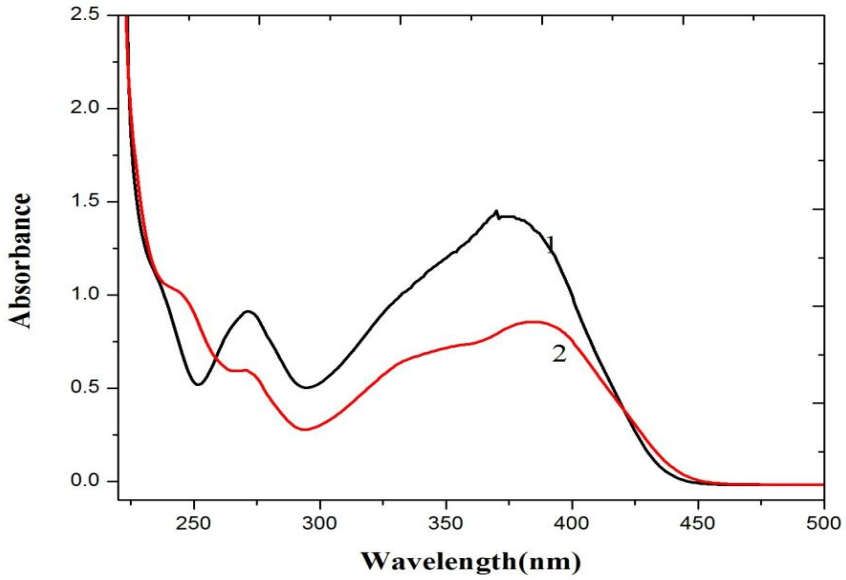

Fig. 7.6. Electronic spectrum of the ligands 1 and 2

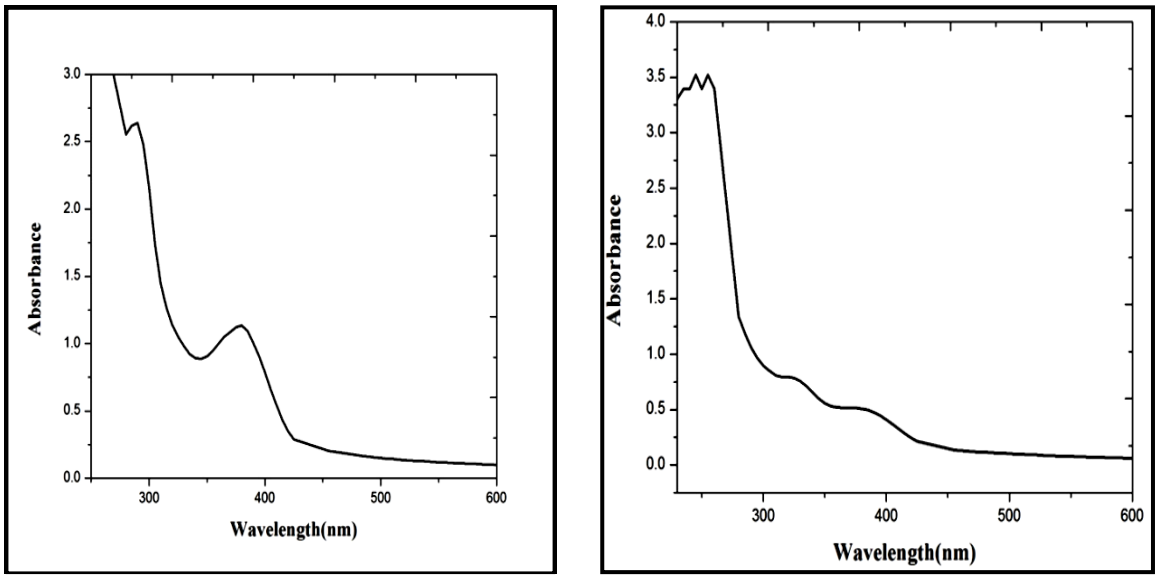

(a) **(b)**

Fig. 7.7. Electronic spectra of Ru(III) complexes 3 and 4

7.3.6. Magnetic susceptibility

Magnetic susceptibility measurements were carried out at room temperature for the complexes. The μ_{eff} values were obtained in the range of 1.58–1.81 BM which corresponds to a single unpaired electron in low-spin d^5 configuration and confirmed the +3 oxidation state of ruthenium in the complexes. Further, the μ_{eff} values suggest an octahedral environment around ruthenium(III) ion in the low-spin d^5 configuration.

7.3.7. EPR spectroscopic analysis

The EPR spectra of the complex have been recorded in the solid state at room temperature. A representative EPR spectrum of complex **3** has been exhibited in Fig. 7.7. The spectra showed no hyperfine splitting due to the interaction with any other nuclei present in the complexes. The complexes have exhibited a single isotropic resonance with 'g' values ranging from 1.99 to 2.12. Although some distortions were found in the octahedral geometries of the complexes, the observation of isotropic lines in the EPR spectra may be due to intermolecular spin exchange and due to the occupancy of the unpaired electron in a degenerate orbital. The observed EPR spectra were in good agreement with some previous reports on ruthenium (III) complexes with some other type ligands.

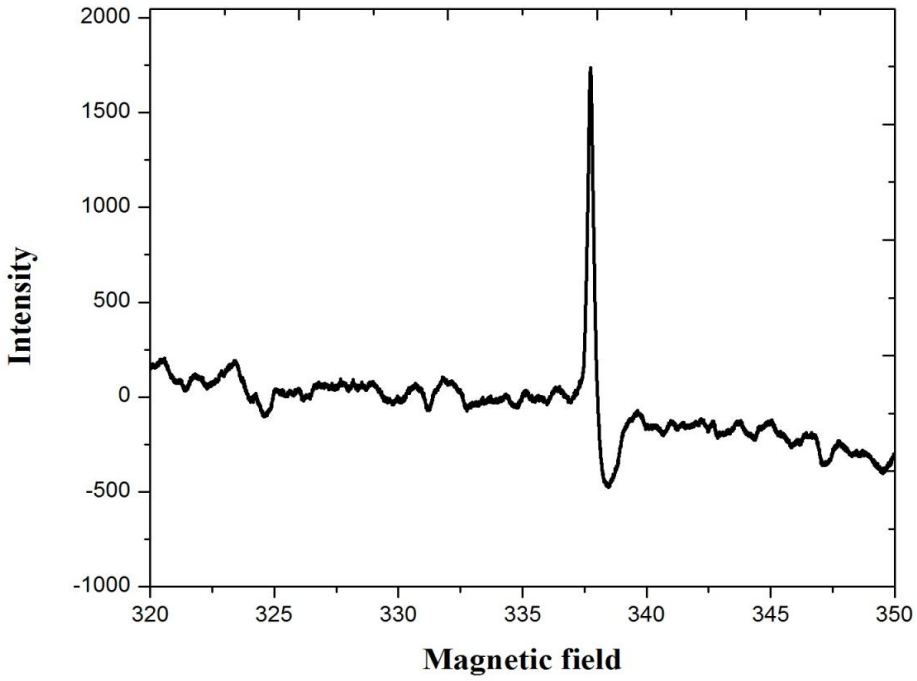

Fig. 7.8. ESR spectrum of complex **3**

7.3.8. EDX Analysis

The proposed geometry of the complexes (Fig. 7.9) is further confirmed from the EDX analysis. The weight percentage distribution of the elements of Ru(III) complexes is given in Table 7.5 and the EDX spectra is given in Fig.7.10a and 7.10b respectively.

Table 7.5. Weight percentage distribution of the elements of Ru(III) complexes

Element	3		4	
	% Calcd	% EDX	% Calcd	% EDX
C	56.49	56.32	50.78	50.61
S	4.57	4.39	4.11	3.98
N	3.99	3.78	3.59	3.42
Ru	14.34	14.12	12.83	12.63

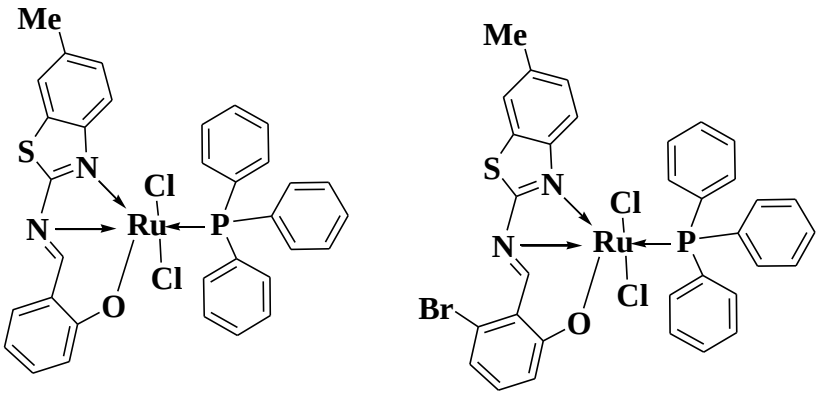

Fig. 7.9. Proposed geometry of the complexes

7.3.9. SEM images

The surface analysis of the Schiff base was examined at different magnifications by scanning electron microscope using Hitachi instrument. The surface morphology of the Schiff bases have been illustrated by using SEM images (Fig. 7.11a and 7.11b). The compound **1** shows needle shaped crystals and compound **2** shows agglomeration of needle shaped structures. The compound **1** is more crystalline than **2.**

The SEM images of the synthesized complexes **3** and **4** are shown in Fig. 7.11c and 7.11d respectively. The images show needle shaped thin rod like structures for complex **3** and round shaped clusters for complex **4.** The sizes of the particles are 834.62 nm for **3** and 404.97 nm for **4.** There are rods with size 252.98 nm and 344.09 nm in the cluster. The rods or the round shaped ball like structures are not hollow. If such type of hollow tubes could be obtained from any synthetic methods in future, it can be a nano carrier in biomedical applications.

7.4. Sensor applications of Schiff bases

Recognition and sensing of heavy and transition metal ions are of considerable current interest in supramolecular chemistry because of their significant importance in chemical, biological, and environmental assays. Commonly employed laboratory methods such as atomic absorption spectrometry, inductively coupled plasma mass spectroscopy, spectrophotometry , neutron activation analysis , anodic stripping voltammetry , X-ray fluorescence spectrometry, electro-thermal, atomic absorption spectrometry, atomic fluorescence spectrometry, cold vapour atomic absorption spectrometry, potentiometric ion-selective electrode, have been established which are of time consuming and high cost. In particular, fluorescent sensors in this regard are of interest due to its easy operational techniques, high sensitivity and of course real time response. Mercury is by far the most toxic and hazardous pollutant among heavy metal ions. Methylmercury is another form of mercury produced from activities of sulphate reducing bacteria and is a potent neurotoxin. Methylmercury causes serious health problems destroying central nervous and endocrine systems causing severe cardiac and motion disorder. The multiple channels of spreading mercury through air and water causes serious problems as it persists in the environment and enters into the food chain. Hence, considerable effort has been devoted to the selective and efficient detection of Hg^{2+} ion. Recently, many sensitive fluorescent probes based on rhodamine, squaraine, benzothiazole derivatives, as well as other fluorophores, have been developed to detect mercury ion. However, many of these systems display short-comings in practical use, such as lack of aqueous solubility, cross-sensitivities towards other metal ions, short emission wavelength and weak fluorescence intensity; only few of them are competitive in terms of sensitivity, selectivity and measurements in aqueous medium. As a result, developing new and practical sensor systems for Hg^{2+} and also for other metal ions is still a challenge.

To check with the chemosensor applications of the synthesized Schiff bases, the metal ions Na^{+}, Ca^{2+}, Mg^{2+}, Al^{3+}, Ba^{2+}, Fe^{2+}, Ni^{2+}, Cu^{2+}, Zn^{2+}, Hg^{2+}, Pb^{2+}, Cd^{2+} and Cr^{3+} were added as their nitrate and chloride salts for the fluorescence spectroscopic experiments. Stock solutions of metal ions (1×10^{-3} M) and the Schiff bases **1** and **2** (1×10^{-4} M) were prepared in DMSO–H_2O (90: 10, v/v). These stock solutions were used for different spectroscopic experiments after appropriate dilution. For the absorbance and fluorescence measurements, 1 cm width and 3.5 cm height quartz cells were used. The excitation was carried out at 380 nm for the Schiff bases with 5 nm emission slit widths in the fluorometer. The change of fluorescence

emission spectra of **1** and **2** after the addition of different cations is shown in Fig. 7.12b. Upon addition of Hg^{2+} to the solution of **1**, the weak fluorescence of **1** has selectively and remarkably enhanced with a blue shift from 550 nm to 485 nm ($\Delta\lambda$ = 65 nm). The discriminating enhancement with the blue shift of the wavelength upon the addition of the Hg^{2+} ion is due to chelation with the Schiff base **1**, a photoinduced electron transfer (PET) from the nitrogen of benzothiazole to the phenyl fluorophore of **1** may be responsible for the preliminary feeble fluorescence of receptor. This enhancement of fluorescence intensity was attributed to the formation of a strong complex between **1** and Hg^{2+}, which inhibited the conformational isomerization of **1** in the excited state.

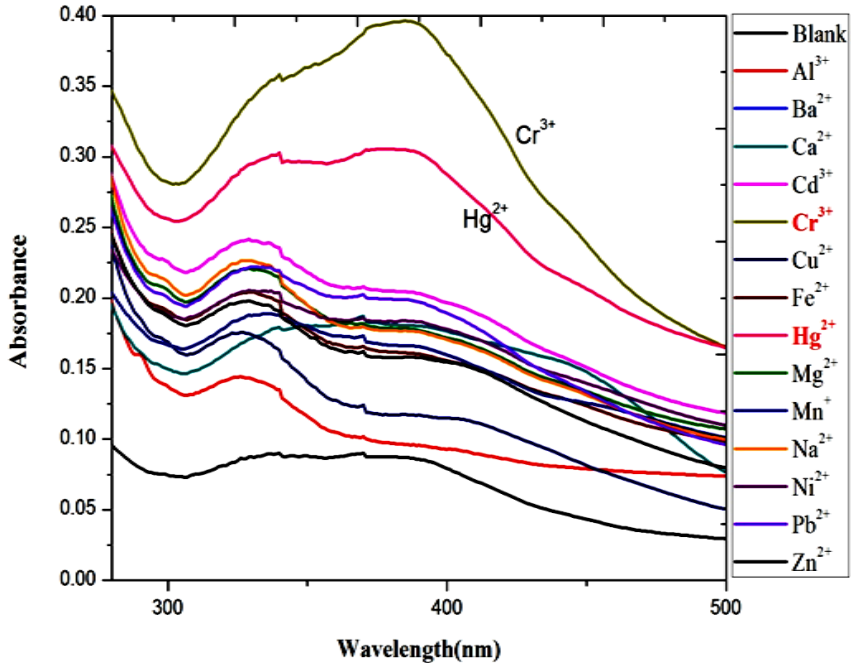

Fig. 7.12a. UV-visible spectra of 1 upon the addition of different metal ions in DMSO– H_2O (9 : 1, v/v) solvent system.

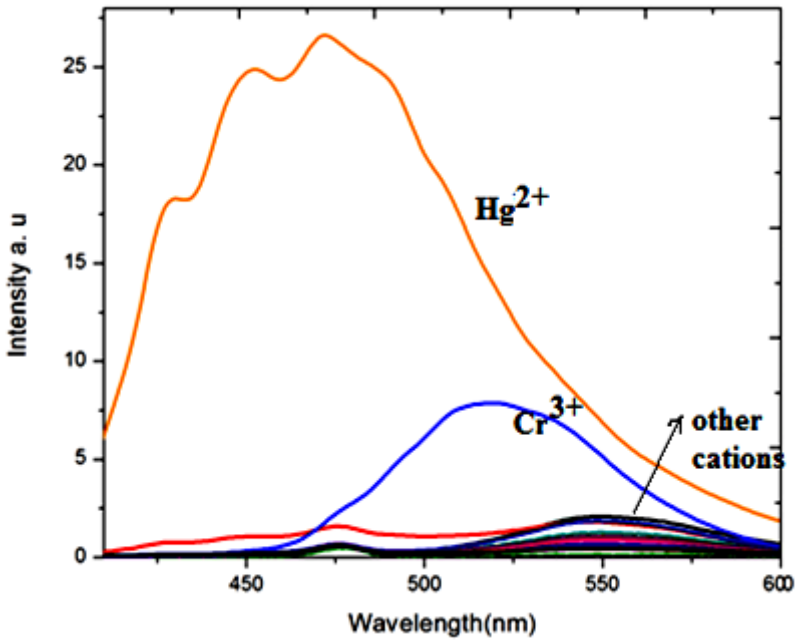

Fig. 7.12b. Fluorescence emission spectra of 1 (10 µM) in the absence and presence of 5 equivalents of various metal ions in DMSO–H_2O (9: 1, v/v) solution.

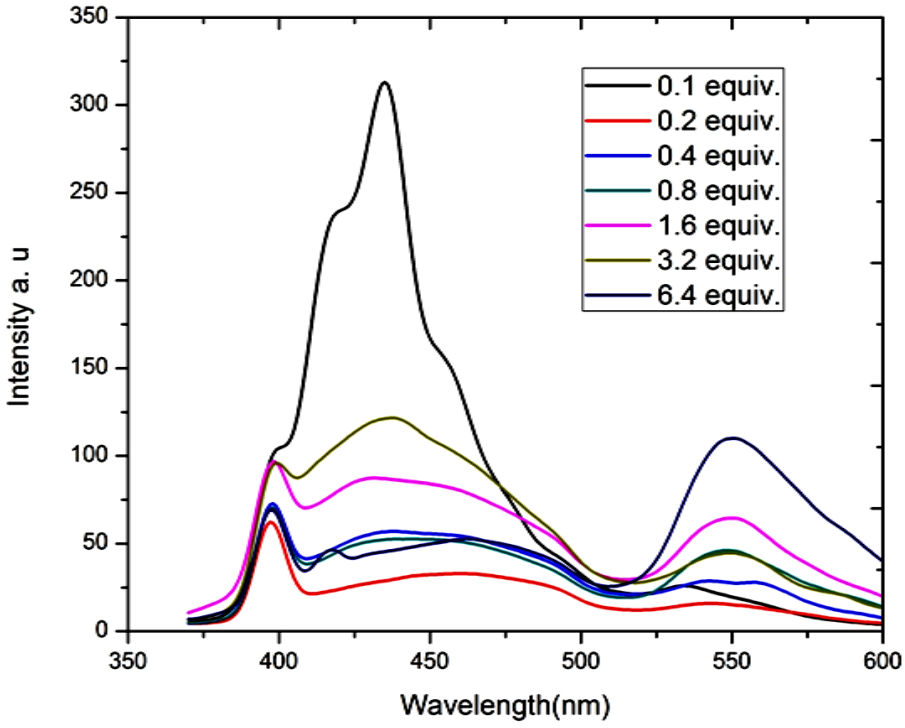

Fig. 7.12c. Fluorescence spectra of 1 (1×10^{-4} M) upon incremental addition of Hg^{2+} (1×10^{-3} M) in DMSO–H_2O (9 : 1, v/v).

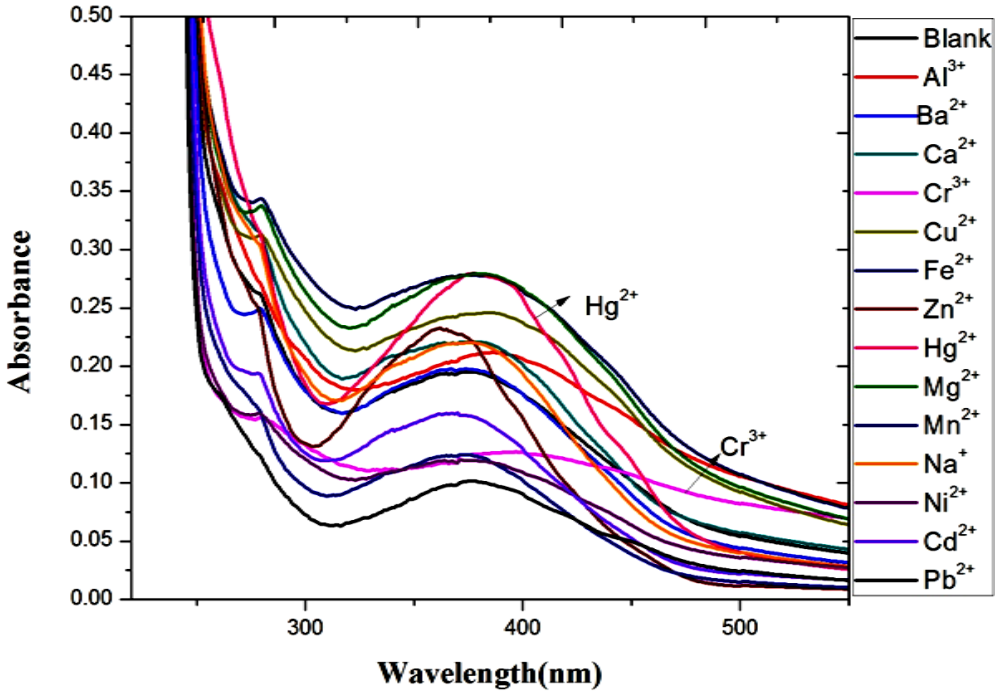

Fig. 7.12d. UV-visible spectra of 2 upon the addition of different metal ions in DMSO– H_2O (9 : 1, v/v) solvent system.

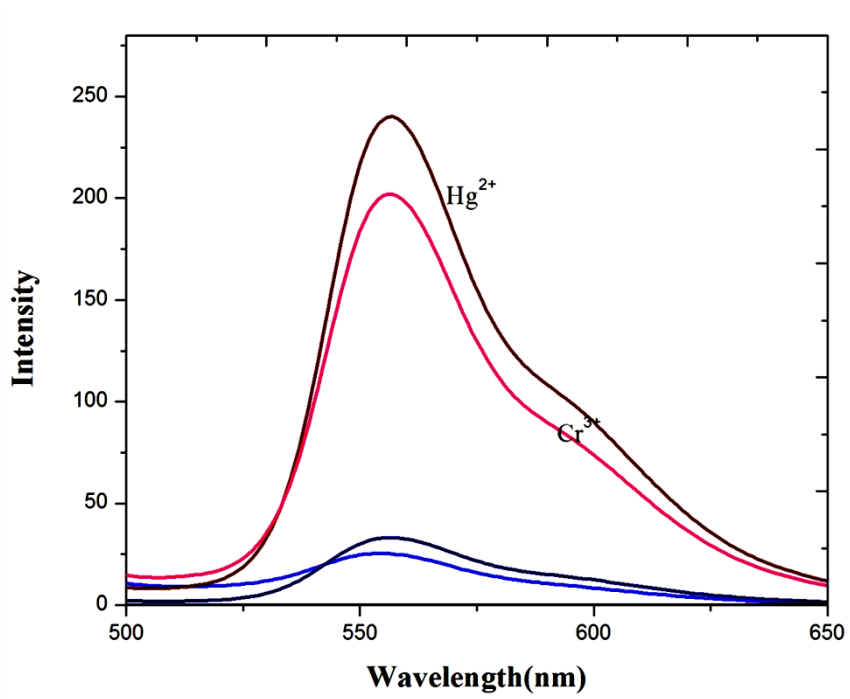

Fig. 7.12e. Fluorescence emission spectra of 1 (10 µM) in the absence and presence of 5 equivalents of various metal ions in DMSO–H_2O (9: 1, v/v) solution.

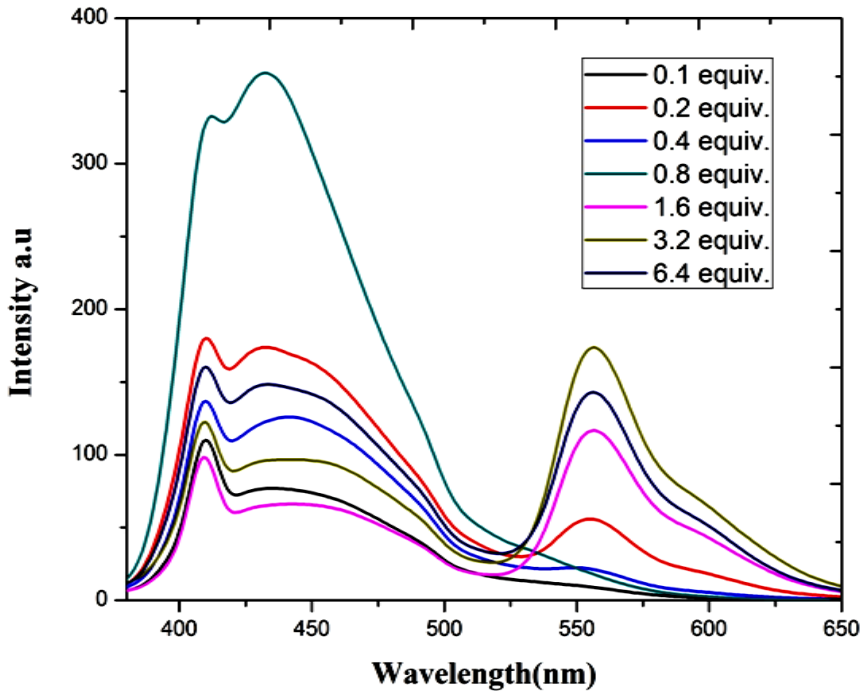

Fig. 7.12f. Fluorescence spectra of 2 (1×10^{-4} M) upon incremental addition of Hg^{2+} (1×10^{-3} M) in DMSO–H_2O (9 : 1, v/v).

In a similar way, the Schiff base **2** also form a strong complex with Cr^{3+} and Hg^{2+} metal ions. This can be visualized from the enhancement of the particular peaks in the fluorescence emission spectrum. The spectras are shown in Figs. 7.12d to 7.12f. As shown in the above figures, the UV-visible absorption spectra of the Schiff bases showed Hg^{2+} selective spectral changes: the addition of Hg^{2+} ions resulted in significant shift of absorption band while those of the other metal ions remained nearly unchanged except for a little change for Cr^{3+} ions.

7.5. Pharmacology

7.5.1. In-vitro antimicrobial activity

Antimicrobial activity of the newly synthesized compounds was tested against *Pseudomonas aeroginosa, Aeromonas hydrophila, Thiobacillus thidurance, Serratia marcescens, Acinetobater baumauii, Aspergillus niger* and *Candida tropicalis.* The results illustrated in Fig. 7.13a revealed that among the tested compounds none had superior antimicrobial activity than the standard antibiotics. However in most of the cases they possess 50% of the activity of standards. Compound **1** and **2** showed pronounced activity against *Pseudomonas aeroginosa*. **1** showed a good activity against *Aeromonas hydrophila, Thiobacillus thidurance* and *Aspergillus niger*. **1**

showed a moderate activity against all the other test organisms. Compound **2** showed a better activity against all the test organisms than **1.**

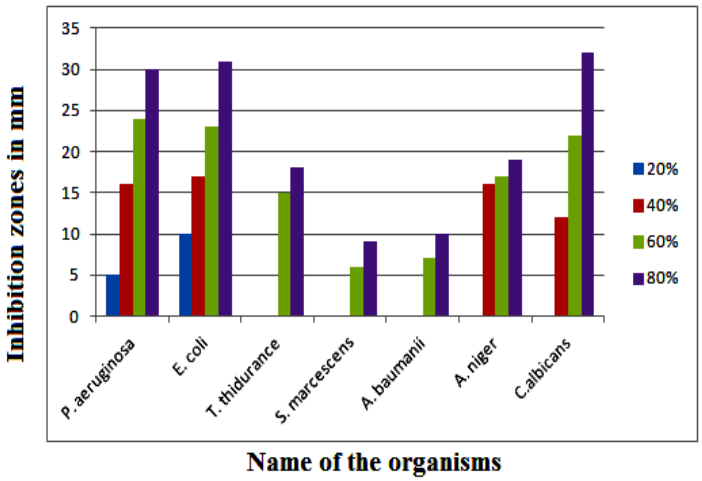

Fig.7.13a. Antimicrobial activity for 1

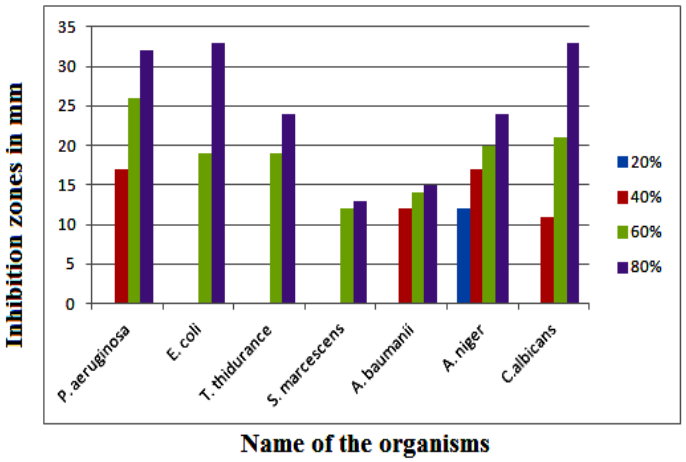

Fig.7.13b. Zone of inhibition in mm for 2

The difference in the two compounds lies in the bromo substituent. So the presence of bromo substituent in **2** brings a pronounced increase in activity[20, 21]. The minimum inhibitory concentration was determined by serial dilution technique. Table 7.6 shows the minimum inhibitory concentration of **1** and **2** against *P. aeruginosa*, *E. coli* and *C. albicans* are 250, 62.5, 250µg/ml and 250, 62.5 and 125µg/ml respectively (Table 7.6).

Table 7.6. MIC values for 1 and 2

S.No	Organisms	1000 µg/ml	500 µg/ml	250 µg/ml	125 µg/ml	62.5 µg/ml	31.25 µg/ml	15.625 µg/ml
				Schiff base 1				
1.	*P. aeruginosa*	-	-	-	+	+	+	+
2.	*E .coli*	-	-	-	-	-	+	+
3.	*C. albicans*	-	-	-	+	+	+	+
				Schiff base 2				
1.	*P. aeruginosa*	-	-	-	+	+	+	+
2	*E. coli*	-	-	-	-	-	+	+
3	*C. albicans*	-	-	-	-	+	+	+

Table 7.7. MIC Values for 3 and 4

S.No	Organisms	1000 µg/ml	500 µg/ml	250 µg/ml	125 µg/ml	62.5 µg/ml	31.25 µg/ml	15.625 µg/ml
				Ru(III)complex 3				
1.	*P. aeruginosa*	-	-	-	-	+	+	+
2.	*E. coli*	-	-	-	-	-	-	+
3.	*C. albicans*	-	-	-	-	-	+	+
				Ru(III) complex 4				
1.	*P. aeruginosa*	-	-	-	-	+	+	+
2	*E. coli*	-	-	-	-	-	-	+
3	*C. albicans*	-	-	-	-	-	+	+

The MIC values of the synthesized complexes have been reported and are shown in Table 7.7. The minimum inhibitory concentration of **3** and **4** against *P. aeruginosa*, *E. coli* and *C. albicans* are 125, 31.25, 62.5 µg/ml and 125, 31.25 and 62.5 µg/ml respectively. The synthesized complexes show a pronounced activity than the ligands. This can be explained based on chelation theory.

7.5.2. In-vitro anticancer activity

Developing effective anti-neoplastic drugs for the clinical therapy of tumor is a hard and vital task for a long time. The clinical success of cisplatin for treating most aggressive solid tumors pioneered the extensive researches of platinum based complexes as the antitumor reagents. However, platinum based chemotherapeutic agents acting by binding covalently to deoxyribonucleic acid (DNA) are severely affected by their serious side effects, such as general toxicity and acquired drug resistance. Thus, developing effective, target specific, less toxic, and preferably non-covalently binding anticancer drugs for treating chronic diseases is an important challenge for chemists in the area of medicinal chemistry. In this regard, the Schiff bases were evaluated for their cytotoxicity against human breast cancer cell line MCF-7 by means of MTT assay method that measures mitochondrial dehydrogenase activity as an indication of cell viability. The results were analyzed by means of cell viability curves and expressed with IC_{50} values in the studied concentration range from 0.1 to 100μM. The activity of the compounds that corresponds to the inhibition of cancer cell growth at a maximum level is shown in Fig. 7.15a. The results of MTT assays revealed that the **2** showed higher cytotoxic effect than **1** which may be due to the presence of bromo substituent in **2.** The IC_{50} values of **1** and **2** are 80.19μM and 44.12μM respectively. The data obtained for our compounds showed cytotoxicity with short incubation period (48h) and hence the data are highly significant[22].

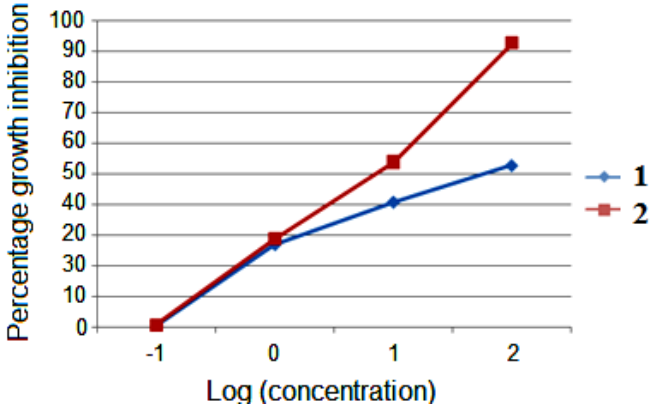

Fig. 7.15a: % Cell viability curves in cytotoxic evaluation of the Schiff bases

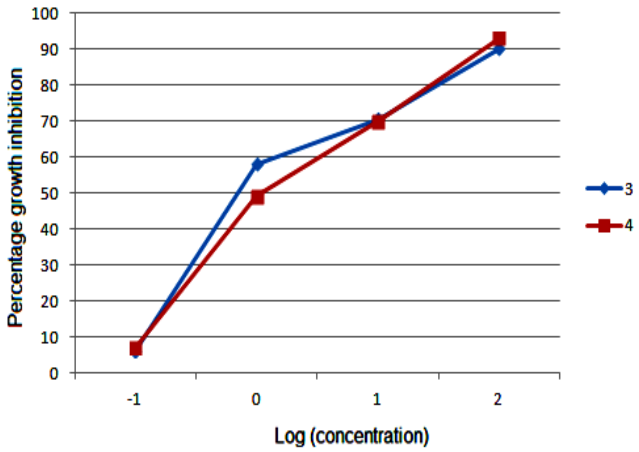

Fig. 7.15b: % Cell viability curves in cytotoxic evaluation of the complexes

The IC_{50} values of the complexes **3** and **4** are 36.85 and 25.68µg/ml respectively. The activity that corresponds to the inhibition of cancer cell growth at a maximum level is shown in Fig.7.15b. The mechanism of action of the ru(III) complexes has been already discussed under section 5.6.2.

7.5.3. DNA Binding Studies

The study of non-covalent interactions of transition metal complexes with DNA is an area of intense current interest. Since DNA is an important cellular receptor many compounds exert their anticancer effects through binding to DNA, thereby changing the replication of DNA and inhibiting the growth of the tumor cells, which is the basis of designing new and more efficient anticancer drugs, where their effectiveness depends on the mode and affinity of binding. Therefore the binding of the compounds to DNA are considered to be highly important in the development of new anticancer drugs.

Compounds binding through intercalation usually results in hypochromism with or without small red or blue shift, since the intercalative mode involves a strong interaction between the planar aromatic chromophore and the base pairs of DNA. The results of absorption spectra of the compounds **1** and **2** in the absence and presence of CT-DNA are given in Figs. 7.16a and 7.16b respectively. With a fixed concentration of the compounds, UV-visible spectra were recorded with the increasing amount of DNA and the maximum absorption peak of DNA was observed at 260 and 268 nm. Meanwhile, the magnitude of absorbance of the bound Schiff base–DNA was a little greater than the measured value of the simply sum of free DNA and free compound.

This is due to a weak hyperchromism effect arising due to the binding interaction between DNA and the compound[24, 25].

The addition of Schiff bases (10^{-6}mol dm^{-3}) to CT-DNA resulted in a hyperchromic shift of the absorption band at 260 and 268 nm. On the basis of the variations in the absorption spectra of DNA upon binding to compound, equation given below can be utilized to calculate the intrinsic binding constant (K).

$$\frac{A^0}{A - A^0} = \frac{\epsilon_C}{\epsilon_{D-C} - \epsilon_c} + \frac{\epsilon_C}{\epsilon_{D-C} - \epsilon_c} \times \frac{1}{K[Q]}$$

A_0 and A represent the absorbance of DNA in the absence and presence of compound at 260 and 268 nm for compound **1** and **2**, εc and ε_{D-C} are the absorption coefficients of compound and compound–DNA complex respectively. The plot of $A_0/A–A_0$ versus 1/[compound] was constructed by using the absorption titration and linear fitting, yielding the binding constant, K = 2.055 × 10^3 and 1.05× 10^4 mol^{-1} dm^3 for **1** and **2** respectively. The observation of hypochromism is indicative of intercalative mode of binding of DNA to the complexes along with the stabilization of the DNA double helix structure. The magnitude of the hypochromism and red shift depends on the strength of the interaction between the DNA and the complex. The binding constants of the complexes **3** and **4** range from 4.9 X10^5 M^{-1}, 5.1 X10^5 M^{-1} respectively.

7.5.4. Tuberculosis activity

Tuberculosis is an infectious bacterial disease caused by *Mycobacterium tuberculosis*, most commonly affecting the lungs. Treatment of drug resistant TB requires extensive chemotherapy with second line anti-tb drugs, which are costlier than first line drugs and produce severe adverse drug reactions. The emergence of multidrug resistant strains highlighted the need for new drugs for the treatment of tuberculosis[23]. The compounds **1** and **2** were checked for its anti-tuberculosis activity and the results are reported in Table 7.8 and Fig. 7.18.

Table 7.8. Anti-tb results of the compounds **1** and **2**

Compound	**100 µg/ml**	**50 µg/ml**	**25 µg/ml**	**12.5 µg/ml**	**6.25 µg/ml**	**3.12 µg/ml**	**1.6 µg/ml**	**0.8 µg/ml**
1	S	S	S	S	S	R	R	R
2	S	S	S	S	S	S	S	R

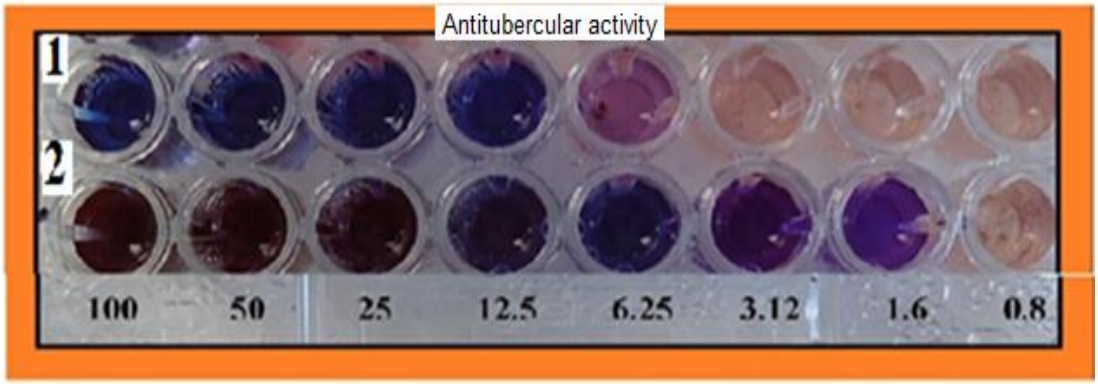

Fig. 7.18. Anti-tuberculosis activity of the compounds

. The strain used for this study was ***M.tuberculosis*** (H37 RV strain) and the standards (MIC values) used were Pyrazinamide (3.125µg/ml) , Streptomycin (6.25µg/ml), Ciprofloxacin (3.125µg/ml). It is obvious from Table 7.8 that **1** shows a moderate activity but **2** has a MIC value of 1.6 µg/ml which is even lower than the tested standards.

7.5.5. Computer aided drug design

Two synthesized Schiff bases **1** and **2** were subjected to docking using Molecular Operating Environment(MOE) program on the 3D structure of the six enzymes, namely, Human Thymidylate Synthase complexed with DUMP and Raltitrex, Crystal structure of Candida Albicans N-MyristoylTransferasepeptidic inhibitor, Catalytic domain of protein kinase pKnb from Mycobacterium tuberculosis in complex with Mitoxantrone, Crystal structure of Topoisomerase atpase inhibitor, Crystal structure of *E. coli* and lactobacillus as dihydrofolatereductase refined at 1.7Å resolution. The study also shows the enzymes interaction with their substrates; 2'-deoxyuridine-5'-monophosphate (DUMP) and methotrexate (MTX)[31, 32]. The glide scores and the E_{model} scores are given in Table 7.9 and the numbers of hydrophobic interactions are given in Table 7.10.

7.5.5.1. Docking on the active site of Thymidylate Synthase

MOE docking studies of the inhibitors were performed using Human thymidylatesynthase (HTS) complexed with DUMP and Raltitrex (PDB ID: 1HVY) as a template. Docking of the Schiff base **1** and **2** (Fig. 7.19a) into HTS active site revealed that hydrogen bond interactions between the –OH in the Schiff base and Glu 87 residue and Arg 215 respectively. Another hydrogen bonding interaction is with –OH of Schiff base **1** and ASN 226 residue. In addition, residues of **1** and **2** show

hydrophobic interactions with the aminoacids Gly 222, Leu 221, Met 311, Ile 108, Tyr 230, Trp 139, Phe 91 and Trp 182, Ala 197, Leu 198 respectively.

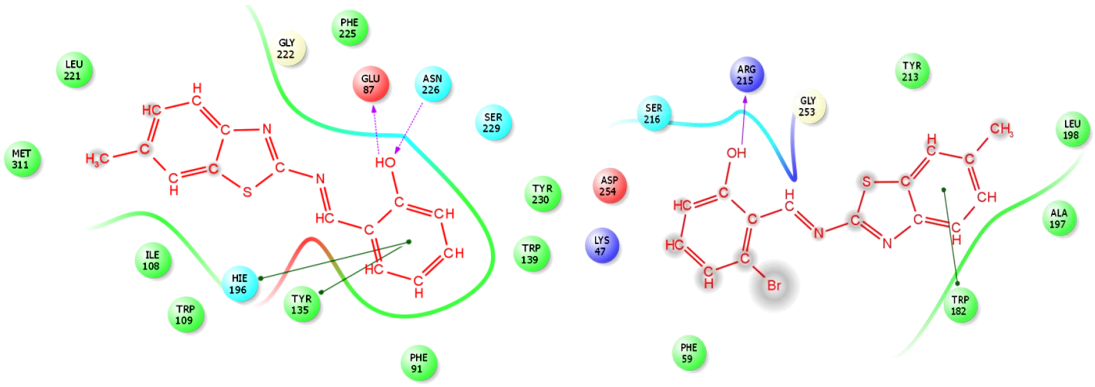

Fig.7.19a. Docking of Schiff bases **1** and **2** into the active site of HTS

7.5.5.2. Docking with the active site *Candida albicans N-MyristoylTrans* inhibitor

MOE docking studies of the inhibitors were performed using crystal structure of Candida albicans N-Myristoyltranferasepeptidic inhibitor (PDB ID: 1VL) as a template.

Docking of Schiff bases **1** and **2** (Fig 6.19b) with 1VL revealed that the hydrogen bond interactions beside hydrophobic interactions were considered to be responsible for the observed affinity as it acts as a hydrogen bond donor to the backbone Trp 85 and Thr 87 residue respectively. **1** acts as a hydrogen bond acceptor to Arg 199 residue. They also exhibit many hydrophobic interactions with various amino acid residues: Thr 87, Glu 84, Ser 86, Arg 198, Val 139, Glu 195 and Ser 86, Arg 142, Gly 147, Glu 98, Leu 94, Glu 95, Leu 88 respectively.

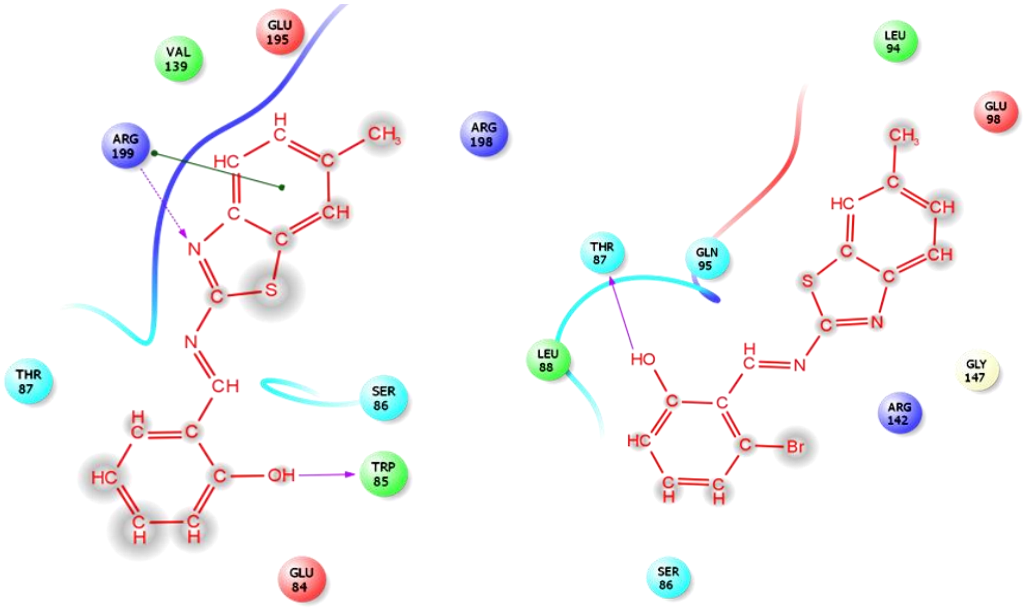

Fig.7.19b. Docking of Schiff base **1** and **2** into the active site of N-Myristoyltransferase

7.5.5.3. Docking with the active site protein kinase pKnb from Mycobacterium tuberculosis

MOE docking studies of the inhibitors were performed using catalytic domain of protein kinase pKnB from *Mycobacterium tuberculosis* in complex with Mitoxantrone (PDB ID: 2FUM) as a template. Docking of Schiff bases **1** and **2** (Fig. 7.19c) with protein kinase pKnB revealed the presence of hydrogen bond interaction between the hydroxyl group of both the Schiff bases , as it acts as a hydrogen bond donor and the side chain residue Val 95. There is also hydrophobic interaction with the amino acid residues Phe 157, Ala 63, Val 72, Met 92, Met 155, Thr 94, Met 145, Val 25 as shown in Fig. 7.19c.

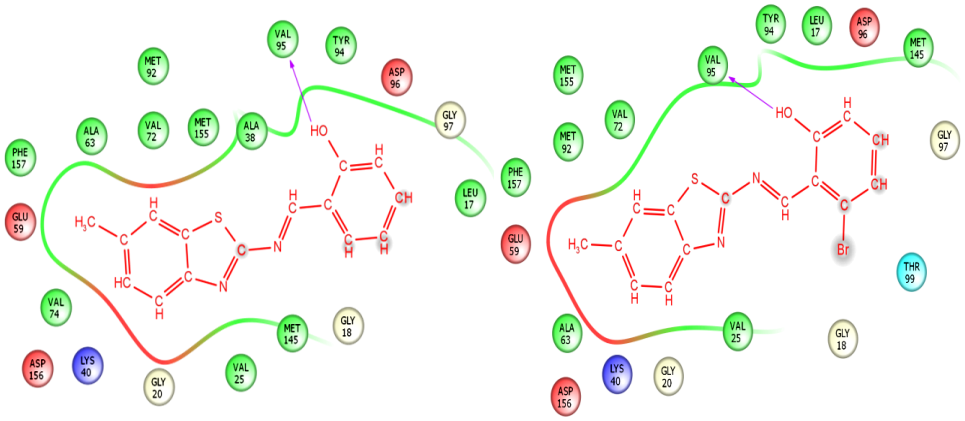

Fig. 7.19c. Docking of Schiff base 1 and 2 into the active site of protein kinase pKnb

7.5.5.4. Docking with the active site Pare

MOE docking studies of the inhibitors were performed using Pare (PDB ID: 3LPS) as a template.Docking of the Schiff bases **1** and **2** (Fig. 7.19d) into the active site revealed the presence of several molecular interactions which were considered to be responsible for the observed affinity of the compound; the hydroxyl atom of the hydroxyl group in the Schiff bases **1** and **2** acts as a hydrogen bond donor to the side chain residue Gly 117 and Asp 113 respectively. In addition to the hydrogen bond interactions in **1** and **2**, many hydrophobic interactions were observed between benzothiazole moiety, phenyl ring and the following amino acid residues: Val 111, Leu 192, Met 118, Val 143, Val 83, Ser 87 and Pro 119, Met 115, Val 143, Ile 134, Leu 192, Val 83, Val 111, Ser 87, Thr 190, Arg 116, Arg 159 respectively.

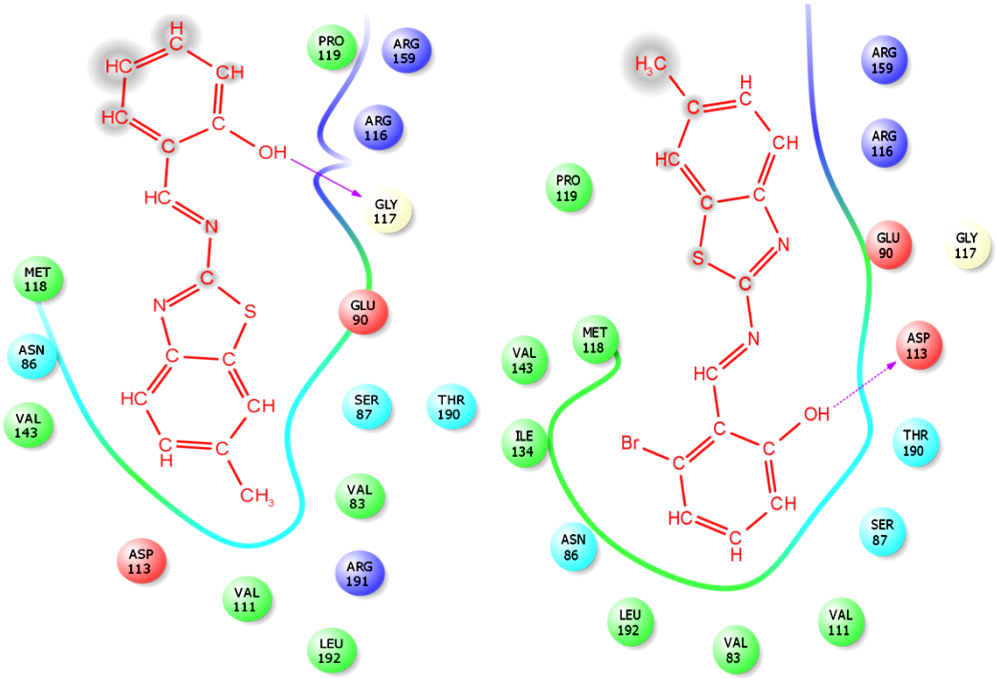

Fig. 7.19d. Docking of Schiff base 2 into the active site Pare

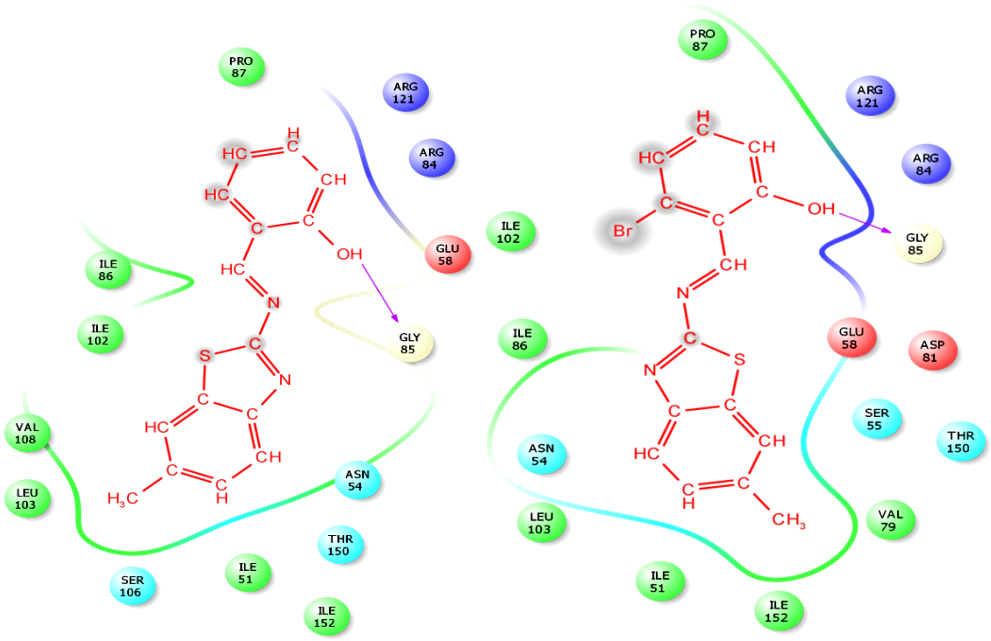

Fig. 7.19e.Docking of Schiff base 1 and 2 into the active site Topoisomerase ATPase

7.5.5.5. Docking with the active site Topoisomerase ATPase inhibitor

MOE docking studies of the inhibitors were performed using crystal structure of Topoisomerase ATPase inhibitor (PDB ID: 3TTZ) as a template. Docking of the Schiff bases **1** and **2** (Fig.6.19e) into active site illustrated the interaction of

hydrogen atom of the hydroxyl group in the Schiff bases as a hydrogen bond donor with the side chain residue Gly 85. Many hydrophobic interactions were also observed between the benzothiazole moiety and benzene ring with many amino acid residues: Pro 187, Ile 86, Ile 102, Val 108, Leu 103, Ser 106, Ile 51, Thr 150 and Pro 87, Ile 102, Ile 86, Leu 103, Ile 51, Ile 152, Val 79 respectively.

7.5.5.6. Docking with the active site E.coli and lactobacilluscasdihydrofolate reductase

MOE docking studies of the inhibitors were performed using crystal structure of *E. Coli* and *lactobacillus* as dihydrofolatereductase (PDB ID:4FDR) as a template. Docking of the Schiff bases **1** and **2** (Fig. 7.19f) into active site revealed that several molecular interactions were considered to be responsible for the observed affinity, as O of the hydroxyl group of the Schiff base acts as hydrogen bond donor with the side chain residue Tyr 100. The phenyl ring acts as both hydrogen bond donor and acceptor with Phe 31 residue. Moreover the hydrophobic interactions were observed with the following amino acid residues: Met 16, Ile 14, Ala7, Ala 6, Ile 94, Ile 50, Leu 54, Leu 28. Fig. 6.20 shows the crystal structure of the active sites used for docking.

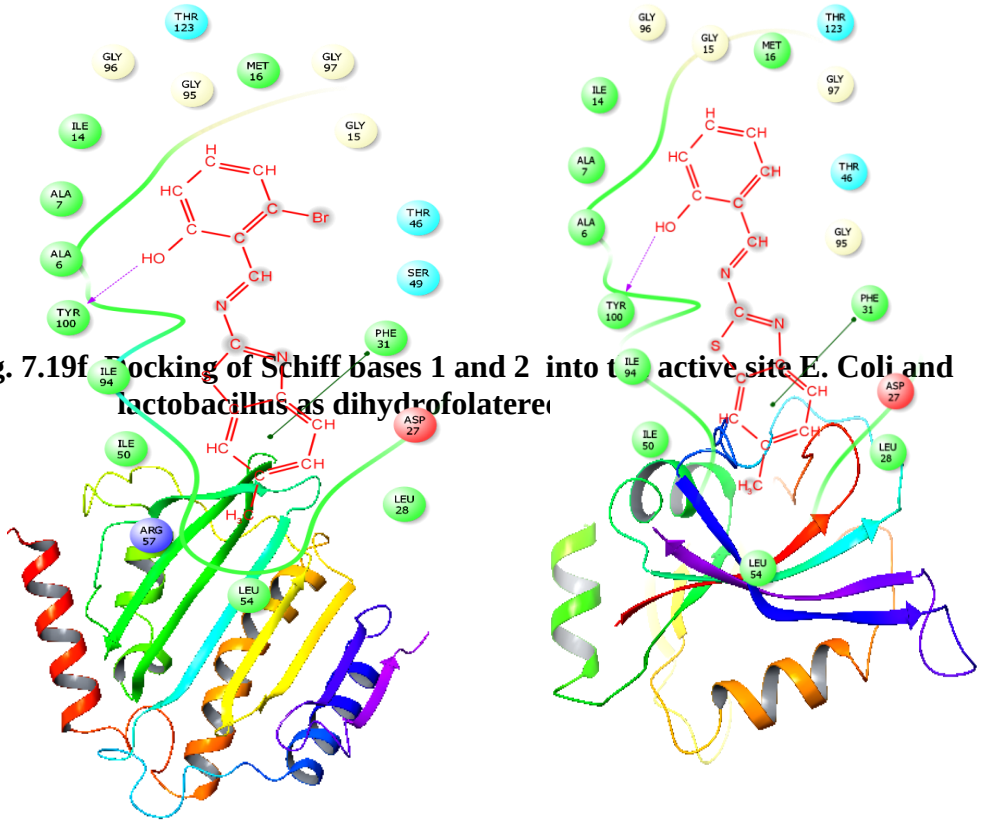

Fig. 7.19f Docking of Schiff bases 1 and 2 into t active site E. Coli and lactobacillus as dihydrofolatere

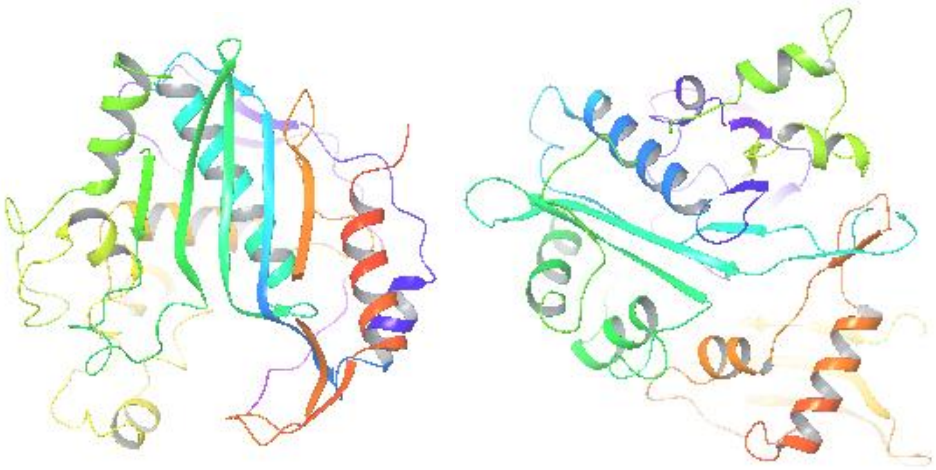

PDB ID: 1HVY **PDB ID: 1VL**

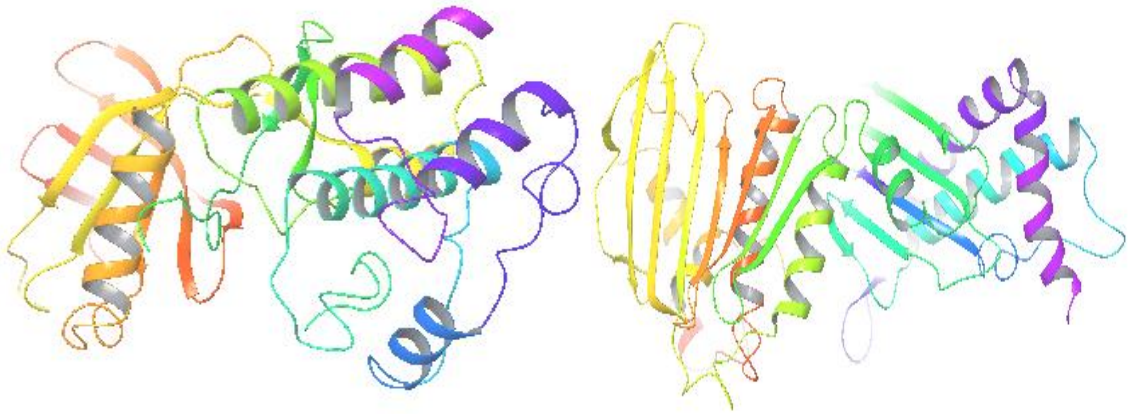

PDB ID: 2FUM **PDB ID: 3LPS**

Fig. 7.20. Crystal structure of the active sites used for docking

7.6. Conclusion

This chapter includes the synthesis, characterization and biological evaluation of the Ru(III) complexes of benzothiazole Schiff bases. The characterization of the ligands and the complexes were characterized using various spectral techniques like FT-IR, UV-visible, EPR, and SEM-EDAX. The sensor application of the Schiff bases has been studied and the ligands are selective towards Hg^{2+} ions which were confirmed using absorption and fluorescence spectral measurements. The biological activity of the ligand and the complexes has been studied and the activity is higher for the complexes. The *in-vitro* anticancer activity of the complexes **3** and **4** showed IC_{50} value of 36.85 and 25.68 µg/ml respectively. The binding ability of the ligands and the complexes with CT-DNA were studied using absorption and fluorescence spectral measurements and the mode of binding is through electrostatic binding for ligands and intercalative mode for the complexes. The molecular docking of the Schiff bases was done against six different active sites

like Human Thymidylate synthase complexed with Dump and Raltitrex, crystal structure of Candida Albicans N-Myristoyl transferase peptidic inhibitor, catalytic domain of protein kinase pKnb from Mycobacterium tuberculosis in complex with Mitoxantrone, Crystal structure of Pare, crystal structure of Topoisomerase atpase inhibitor, crystal structure of E. coli and lactobacillus casdihydrofolate reductase. These synthesis of the complexes throw light on some of the applications of it for future research.

References

1. Patel N B, Shaikh F M, *Sci Pharm*, 78 (2010) 753.
2. Ha S, Koh T, Ong S, Lee T, Sivasothy Y, *Molbank* M609 (2009) 1.
3. Soni B, Ranawat M S, Sharma R, Bhandari A, Sharma S, *Eur J Med Chem,* **45** (2010) 2938.
4. Shafi S, Alam M M, Mulakayala N, Mulakayala C, Vanaja G, Kalle A M, Pallu R, Alam M S, *Eur J Med Chem,* **49** (2012) 324.
5. Bhavsar D, Trivedi J, Parekh S, Savant M, Thakrar S, Bavishi A, Radadiya A, Vala H, Lunagariya J, Parmar M, Paresh L, Loddo R, Shah A, *Bioorg Med Chem Lett,* **21** (2011) 3443.
6. Delmas F, Avellaneda A, Giorgioetal C D, *Eur J Med Chem,* **39** (2004) 685.
7. Pereira G A, Massabni A C, Castellano E E, *Polyhedron* **38** (2012) 291.
8. Burger A, Sawhey S N, *J Med Chem,* **11** (1968) 270.
9. Sharpe T R, Cherkofsky S C, Hewes W E, Smith D H, Gregory W A, Haber S B, Leadbetter M R, Whitney J G, *J Med Chem,* **28** (1985) 1188.
10. Amir M, Asif S, Ali I, Hassan M Z, *Med Chem Res,* **21** (2012) 2661.
11. Kashiyama E, Hutchinson I, Chua M S, Stinson S, Phillips L R, Kaur G, Sausville E A, Bradshaw T D, Westwell A D, Stevens M F G, *J Med Chem*, **42** (1999) 4172.
12. Karalı N, Guzel O, Ozsoy N, Ozbey S, Salman A, *Eur J Med Chem,* **45** (2010) 1068.
13. Chaudhary P, Sharma P, Sharma A, Varshney J, *J Curr Pharm Res*,**2** (2010) 5.
14. Rana A, Siddiqui N, Khan S A, *Indian J Pharm Sci*, **69** (2007) 10.
15. Malik J, Manvi F V, Nanjwade B K, Purohit P, *J Pharm Res,* **2** (2009) 1687.
16. Malik J K, Manvi F V, Nanjwade B K, Singh S, Purohit P, *Der Pharm Lett,* 2 (2010) 347.
17. Sharma N K, Jha K K, *Int J Curr Pharm Res,* **2** (2010) 1.

18. Issa R M, Khedr A M, Rizk H, *J Chin Chem Soc*, **55** (2008) 875.
19. Sampath K, Sathiyaraj S, Jayabalakrishnan, *Bull Korean Chem Soc*, **34** (2013) 367.
20. Chohan Z H, Scozzafava A, Suparan C T, *J Enzyme Inhib Med Chem*, **18** (2003) 259.
21. Vicini P, Geronikaki A, Incerti M, Busonera B, Poni G, Alba Cabras C, La Colla P, *Bioorg Med Chem*, **11** (2003) 4785.
22. Navin B, Shaikh F M, *Saudi Pharm J*, **18** (2010) 129.
23. Prabhu P, Paneerselvam T, Shastry C S, Sivakumar A, Pande S S, *J Saudi Chem Soc*, **19** (2015) 181.
24. Radwan A A, Abdel-Mageed W M, *Molecules*, **19** (2014) 2247.
25. Alizadeh R, Afzal M, Arjmand F, *Spectochimica Acta Part A: Mol Biomol spectros*, **131** (2014) 625.
26. Alizadeh R, Yousuf I, Afzal M, Srivastav S, Srikrishna S, Arimand F, *J Photochem Photobiol B*, **143** (2015) 61.
27. Raman N, Sobha S, Mitu L, *J Saudi Chem Soc*, **17** (2013) 151.
28. Chandrasekaran S, Sameena Y, MuthuVijayan Enoch I V, *Turk J Chem*, **38** (2014) 725.
29. Chandrasekaran S, Sameena Y, Muthuvijayan Enoch I V, *Australian J Chem*, **67** (2013) 256.
30. Chandrasekaran S, Sudha N, Premnath D, Enoch I V, *J Biomol Struct Dyn*, **8** (2014) 1.
31. Yousuf S, Radhika D, Enoch I V, Easwaran M, *Spectrochimica Acta A Mol Biomol. Spectrosc.* **98** (2012) 405.
32. Ravichandiran P, Premnath D, Vasanthakumar S, *J Chem Biol*, **7** (2014) 122.
33. Ravichandiran P, Jegan A, Premnath D, Vasanthakumar S, *Spectrochimica Acta A Mol Biomol. Spectrosc*, 12 (2014) 477.